Journal of
Applied Remote Sensing

RemoteSensing.SPIEDigitalLibrary.org

Above-ground biomass estimates based on active and passive microwave sensor imagery in low-biomass savanna ecosystems

Andreas Braun
Julia Wagner
Volker Hochschild

SPIE.

Andreas Braun, Julia Wagner, Volker Hochschild, "Above-ground biomass estimates based on active and passive microwave sensor imagery in low-biomass savanna ecosystems," *J. Appl. Remote Sens.* **12**(4), 046027 (2018), doi: 10.1117/1.JRS.12.046027.

Above-ground biomass estimates based on active and passive microwave sensor imagery in low-biomass savanna ecosystems

Andreas Braun,[a,*] Julia Wagner,[b] and Volker Hochschild[a]
[a]University of Tübingen, Department of Geosciences, Institute for Geography, Tübingen, Germany
[b]Stockholm University, Department of Physical Geography, Stockholm, Sweden

Abstract. Although many studies exist on the estimation and monitoring of above-ground biomass (AGB) of forest ecosystems by methods of remote sensing, very little research has been carried out for ecosystems of low primary production, such as grasslands, steppes, or savannas. Our study intends to approach this gap and investigates the correlation between space-borne radar information and AGB at the scale of 10 tons per hectare and below. Additionally, we introduce the integration of passive brightness temperature as an additional covariate for biomass estimation, based on the hypothesis that it contains information complementary to microwave backscatter of the active sensors. Our findings show that large-scale estimates of AGB can be conducted for grasslands and savannas at high accuracy (R^2 up to 0.52). Additionally, we found that the integration of passive radar can increase the quality of AGB estimates in terms of explained variance for selected cases. We hope that these indications are a starting point for more integrated approaches toward biomass estimations based on Earth observation methods.
 [DOI: 10.1117/1.JRS.12.046027]

Keywords: above-ground biomass; synthetic aperture radar; special sensor microwave imager; semiarid landscapes; Sénégal.

Paper 180520L received Jun. 21, 2018; accepted for publication Nov. 13, 2018; published online Dec. 11, 2018.

1 Introduction

Satellite imagery has become the primary source for biomass estimates of regions.[1] It is used for the assessment of agricultural yields,[2–4] monitoring resources over long time periods,[5–7] and forecasting carbon stocks and emissions.[8–10] In particular, the effects of climate change and desertification became a focus of Earth observation in sub-Saharan Africa.[11–13] As grasslands cover nearly one-fifth of the global land surface, their contribution to the carbon stock is expected to be between 10% and 30%.[14,15] And recent studies indicate that especially carbon losses caused by land-use changes and deforestation of African grasslands and savannas are 3 to 6 times larger than previously thought.[16] Monitoring of grassland ecosystems is, therefore, of crucial interest for the evaluation of carbon emissions.[17] The use of synthetic aperture radar (SAR) satellite data has been found to be of special value because of its wavelength and the sensitivity of the signal toward ramified structures and voluminous canopies.[18] A stable relationship between SAR backscatter and above-ground biomass (AGB) has been observed and exploited in numerous studies.[19–24] Many of them report signal saturation between 100 and 250 tons per hectare (t/ha) above which the measured SAR backscatter no longer increases correspondingly.[25,26] To overcome this limit, approaches based on radar polarimetry,[27] multifrequency exploitation,[28] integration of optical[29] or LIDAR data,[30] and SAR interferometry[31] have been proposed. However, while most of the studies are concentrating on tropical and boreal forest biomass, only a few studies deal with biomass estimation in arid or semiarid regions with herbaceous ground layer and sparse vegetation cover.[32–34] This aspect is primarily an

*Address all correspondence to Andreas Braun, E-mail: an.braun@uni-tuebingen.de

outcome of SAR backscatter alone not significantly representing biomass variations below 5 t/ha as well as other surface characteristics, such as roughness and soil moisture, which are superimposing the signal at these levels.[35–37] One further constraint is that coverages of cross-polarized acquisition modes (HV or VH), which are found to be most sensitive toward biomass, are often not large enough to cover whole regions at the same acquisition conditions (date, incidence angle).[38–40]

One way to make use of the sensitivity of microwaves toward different scattering mechanisms is the utilization of sensors that employ different frequencies.[41] While combinations of short and long microwaves have been successfully applied for forest biomass estimates,[42,43] only Srivastava et al.[44] and Herold et al.[45] confirmed their potential for thin vegetation layers. Integrating passive radar for large-scale mapping is mostly limited to soil moisture[46] or surface temperature.[47] Ferrazzoli et al.[48] demonstrated their sensitivity toward vegetation biomass because of the water content plants and also Eom mentions their potential to detect changes in vegetation,[49] but none of these studies created spatial predictions from these data. Only Liu et al.[50] mapped terrestrial biomass between 1993 and 2012 at the global scale based on space-borne passive radar and report an estimated decrease of 0.07 pg C/yr, mostly resulting from deforestation in the tropics, but also because of changes in savannas and shrublands.

In this letter, we propose a method to derive AGB estimates for large parts of Sénégal, ranging between tropical, semiarid, and arid climate zones based on the integrated use of imagery of radar measurements of sensors of different wavelengths. We investigate their contribution for wide-area biomass estimations and want to initiate discussions about the potential for automated long-term monitoring of resources in sub-Saharan African countries.

2 Data and Methods

2.1 *Satellite Data*

Three types of satellite data were used in this study: (1) ENVISAT Advanced Synthetic Aperture Radar (ASAR) as wide Swath (WS) mode products at a spatial resolution of 150 m, (2) Advanced Land Observing Satellite (ALOS) Phased Array L-band Synthetic Aperture Radar (PALSAR) in wide beam (WB) mode products at a spatial resolution of 100 m, and (3) Special Sensor Microwave Imager (SSM/I) in V and H polarizations, representing surface brightness temperature [B_T], at a spatial resolution of 12.5 km.[51] Because of the unavailability of a consistent polarization, SSM/I data were acquired in both horizontally (H) and vertically (V) receiving polarization so that it could be combined with other data of both configurations. Table 1 shows the data used in this study. Using the revisit frequency of SSM/I of one day, a mean raster was calculated for the 31 days of December of the respective year.

Although field data are available for the years 1985 to 2013 (see Sec. 2.2), the selection of satellite imagery was restricted by the availability of images from all three sensors during the dry season. This limited the usable satellite data to the years 2006, 2009, and 2010.

2.2 *Field Data*

Biomass collection was carried out on a yearly base at the time of maximum phytomass, which occurs between the end of September and late October before the seeds are grown. Forty-eight representative sites were selected in Sénégal based on the intersection of topographic and phytogeographic maps (see spatial distribution in Fig. 2, prediction maps). These sites were consistently used for sampling since 1987. Each identified site has a size of 9 km^2 and was divided into nine units of 1 km^2. A collection of biomass data was then conducted within each of these units by identifying homogeneous vegetation patterns (subunits) at the local level. Depending on the vegetation pattern of the subunits (homogenous, gradient, and mosaic), a representative number of stratified measurements was undertaken as described in the following.

For herbaceous units, linear transects of 200 m were drawn, as suggested by Poissonet et al.,[52] and both destructive and nondestructive allometric measures were taken (fr = relative frequency of the layer along the transect, pm = average productive green weight [g/m^2], and

Table 1 Satellite data used in this study.

Sensor	Date	Frequency [GHz]	Polarization
ENVISAT ASAR	December 19, 2006	5.3 (C-band)	HH
ALOS PALSAR	December 23, 2006	1.27 (L-band)	HH
SSM/I	December 2006	85 (W-band)	H
SSM/I	December 2006	85	V
ENVISAT ASAR	December 20, 2009	5.3	VV
ALOS PALSAR	December 31, 2009	1.27	HH
SSM/I	December 2009	91	H
SSM/I	December 2009	91	V
ENVISAT ASAR	November 29, 2010	5.3	VV
ALOS PALSAR	November 18, 2010	1.27	HH
SSM/I	December 2010	91	H
SSM/I	December 2010	91	V

ms = dry matter rate). This allows the characterization of different spatial compositions, such as homogeneous landscapes, gradients, and mosaics. The herbaceous biomass was then calculated by the following equation: $P_H[\mathrm{kg/ha}] = fr * pm * ms * 10$.[53] Vegetation communities in the study area consist of open woodlands, mainly dominated by tree species of the Combretacea (*Combretum collinum*, *Combretum glutinosum*, and *Guiera senegalensis*), Caesalpiniaceae (*Burkea Africana* and *Cordyla pinnata*), Apocynaceae (*Saba senegalensis*), and Fabaceae (*Pterocarpus lucens*) families.[54,55]

Woody biomass of individual trees was determined within squared plots of 50×50 m by measuring their diameter at breast height (DBH, 1.30 m) to be inserted in the following allometric equation: $P_i = a * \mathrm{DBH}^b$, where a and b are constants depending on the tree species.[53] The sum of all trees within a plot determines the woody biomass of an area P_L was then added to the herbaceous biomass P_H to get the full AGB of this area. A detailed description of the data collection methodology is given by Yameogo et al.[53] and the background on the used regressions is documented by Cissé et al.[56] Biomass data used in this study were also used in studies on monitoring sub-Saharan biomass[57] and the establishment pastoral early warning system based on medium resolution optical satellite imagery at a spatial resolution of 1 km.[58]

After the removal of sites with missing values or sites outside the area covered by the satellite imagery, a total number of 63 measurements remained (21 per investigated year) for correlation analysis (see Sec. 2.4) ranging from 740 to 12,380 kg of AGB per hectare [kg/ha] with a mean of 4043, a median of 3183, and a standard deviation of 2730 kg/ha. We additionally calculated Moran's I[59] to test for spatial autocorrelation. The results indicate slight spatial dependencies of AGB (2006: 0.42, 2009: 0.39, and 2010: 0.31), which can be explained by the climatic latitudinal gradient within the study area and the increased continental effects in west–east direction.

2.3 *Data Preparation*

SAR data were radiometrically calibrated to radar brightness (beta naught) by applying the scaling constant as described by Henry et al.[60] and Shimada et al.,[61] respectively. To compensate for topographic variations and their impact on backscatter intensity, incidence angle normalization was performed using the 1 arc second shuttle radar topography mission digital elevation model,[62] resulting in terrain-flattened Gamma naught.[63] Range-Doppler terrain correction was applied to all SAR images to compensate for topographically induced geometric distortions.[64] Backscatter

data were converted to the dB scale for better contrasts in the low-value ranges. SSM/I products were directly used as provided by the NSIDC due to their extensive and accurate internal calibration.[65,66]

All raster processing was performed in the sentinel application platform provided by the European Space Agency (ESA).

2.4 *Correlation Analysis*

To analyze correlations between AGB measured in the field and the radar values from the images, backscatter intensities of ENVISAT and ALOS PALSAR were extracted at the sampling sites within a radius of 1.5 km (about 7 km^2) and averaged to one mean value per SAR sensor and site. Pixels within this radius represent nearly the same area as defined in the sampling process of the field reference data (9 km^2). This grants that both the independent and dependent variable refer to a similar area. Furthermore, the influence of speckle at the local scale is reduced. As for SSM/I data, one radar brightness value is extracted for each sampling site. Although it technically represents a clearly larger area, increasing the representative area of the SAR sensors by the radius of 1.5 km reduced the ratio between the pixel sizes of active radar and passive radar systems used in this study from 1:6000 to 1:22.

The extracted radar values were correlated with the AGB measurements of the corresponding sites and years using an exponential regression in R software package.[67] The relationship between backscatter and AGB is described by an exponential function as $y = a * e^{bx}$, where y represents AGB, x shows the image variables, and a and b are the equation coefficients. Although there are also linear,[23,24] logarithmic,[42] and power law-based[68] approaches, the majority of studies reports best results based on nonlinear exponential regressions, which also reflects our observations.[5,20,28,39,69] Furthermore, the conversion of SAR data to a dB scale already eliminates the logarithmic nature of the relationship between AGB and backscatter intensity.[25]

In addition to the single measurements of each sensor (Table 2, a, b, and d), several recombinations of the different sensor's values were derived to generate a variety of predictors to be inserted as further independent variables of the regression (Table 2, c, e–i). This is based on the assumption that the information retrieved at different wavelengths is complementary for the description of the present biomass. Combining these data for the regression helps to analyze

Table 2 Equations for prediction of AGB from nonlinear regression.

Scatter plot	Sensor or combination	Variable	Regression	R^2_{cd}	Samples	R^2_{val}	RMSE
a	ALOS PALSAR (A)	HH	$25748.06 * e^{0.123 * A\_mean}$	0.332	$n = 63$	0.191	2465.4
b	ENVISAT (E)	HH & VV	$37664.61 * e^{0.181 * E\_mean}$	0.369	$n = 63$	0.231	2370.7
c	ENVISAT and ALOS PALSAR	E-[5*(E/A)]	$79136.86 * e^{0.182 * \{E - [5 * (\frac{E}{A})]\}}$	0.375	$n = 63$	0.325	2431.2
d	SSM/I (S)	H only	$13.1988 * e^{0.001947 * SSM/I_H}$	0.129	$n = 63$	0.061	2612.3
e	ENVISAT and SSM/I	E/S 2006 H	$46335.01 * e^{583.855 * (\frac{E}{S})}$	0.498	$n = 21$	0.257	1569.6
f	ALOS PALSAR and SSM/I	A/S 2006 H	$23196.87 * e^{378.979 * (\frac{A}{S})}$	0.501	$n = 21$	0.229	1599.6
g	ENVISAT and ALOS PALSAR and SSM/I	PC1 2006	$447.734 * e^{-0.007 * PC\_1\_2006}$	0.515	$n = 21$	0.248	1552.7
h	ENVISAT and ALOS PALSAR and SSM/I	PC1 2009	$1456.50 * e^{-0.003 * PC\_1\_2009}$	0.302	$n = 21$	0.172	1547.0
i	ENVISAT and ALOS PALSAR and SSM/I	PC1 2010	$6368.85 * e^{-0.003 * PC\_1\_2010}$	0.341	$n = 21$	0.141	2521.5

how well these joint measures are suitable to improve the prediction accuracy. Furthermore, it helps to overcome the difference in spatial resolution between active and passive radar data by simply extracting the values at similar footprints (see Sec. 2.3) without the need for spatially upsampling or downsampling one of each dataset, which was found to potentially have unwanted side effects on the quality of results.[70–72]

To also create spatial predictor variables that are based on all three input sensors, a principal component analysis (PCA) was conducted as an acknowledged method of sensor combination.[73] However, because active and passive radar produce data of different range and units (see Sec. 2.3), all images were transformed into an eight-bit integer format. Based on these rasters, a PCA was performed for each investigated years using all three satellite scenes available. The first principal component (PC1) of each year was used for the regression analysis (maps g, h, and i), which showed an explained variance of the 0.502 (2006), 0.515 (2009), and 0.418 (2010), respectively. Although the rasters of ALOS and ENVISAT were found to be spatially correlated, the integration of SSM/I data introduced newly emerging patterns in PC1. This integrated spatial representation of all three sensors is believed to contribute to the prediction accuracy of the regressions because it features wavelengths of various sizes that might interact with different parts of the vegetated surface.

To test the strength of the relationship between AGB and the independent variables, the coefficient of determination (R^2_{cd}) was calculated for each regression as shown in Table 2. Greater values indicate a stronger relation, whereas 0 means no correlation between the dependent variable (AGB) and the independent variable (radar information) and 1 meaning that the independent variable can be used to fully explain the variance of the dependent variable.

3 Results and Discussion

3.1 *Statistical Prediction of Above-Ground Biomass*

Figure 1 shows selected scatter plots of the relationship between active and passive radar information, with the measured biomass as shown in Table 2. As all scatter plots show, a strong relationship exists between observed biomass and the layers retrieved from satellite imagery and a clear trend is visible. However, it has to be noted that many more combinations of configurations and derivatives were tested (examples of combinations are presented by Omar et al.[42]) and that the selection shows the variables with the highest correlations that were found.

In general, ALOS and ENVISAT regressions alone already deliver a coefficient of determination (R^2_{cd}) of 0.3 with slightly higher correlation for the ENVISAT. The results indicate that microwaves of shorter wavelength (ENVISAT, $\lambda = 5.6$ cm) are more sensitive toward the roughness and volume of fine vegetation surfaces, such as grasslands or small bushes, while larger wavelengths (ALOS, $\lambda = 23.5$ cm) are partly able to penetrate canopies and ground vegetation layers and typically interact stronger with objects of comparable size, such as large branches or stems of savanna trees.[28,44,45]

As shown in scatter plot c, combining short- and long-wave information of ALOS and ENVISAT potentially increases the significance of the correlation, even if only to a small degree. This can be explained with the observation that horizontally and vertically polarized microwaves interact with different parts of the vegetation layer.[74,75]

For scatter plot d, only SSM/I data were used. It shows that passive radar data alone cannot predict the distribution of AGB to a sufficient degree. Looking at the maps of Fig. 2, the overall distribution is rather inverted compared with the other cases. Additionally, the low spatial resolution of 12.5 km might not be sufficient to represent the spatial scale of biomass variations at the ground. Our assumption, however, is that it can be employed as a complementary source of information to depict patterns that are not fully related to active SAR backscatter measures of ALOS and ENVISAT.

For this reason, we calculated the ratio between active and passive information to be used in the correlation. Plots e and f demonstrate how a combination of both could statistically increase the predictions of AGB. As shown, both regression lines match the measured AGB values quite well, resulting in R^2_{cd}s of 0.49 and 0.50. Especially the high R^2_{cd} of plot f results from the fact that

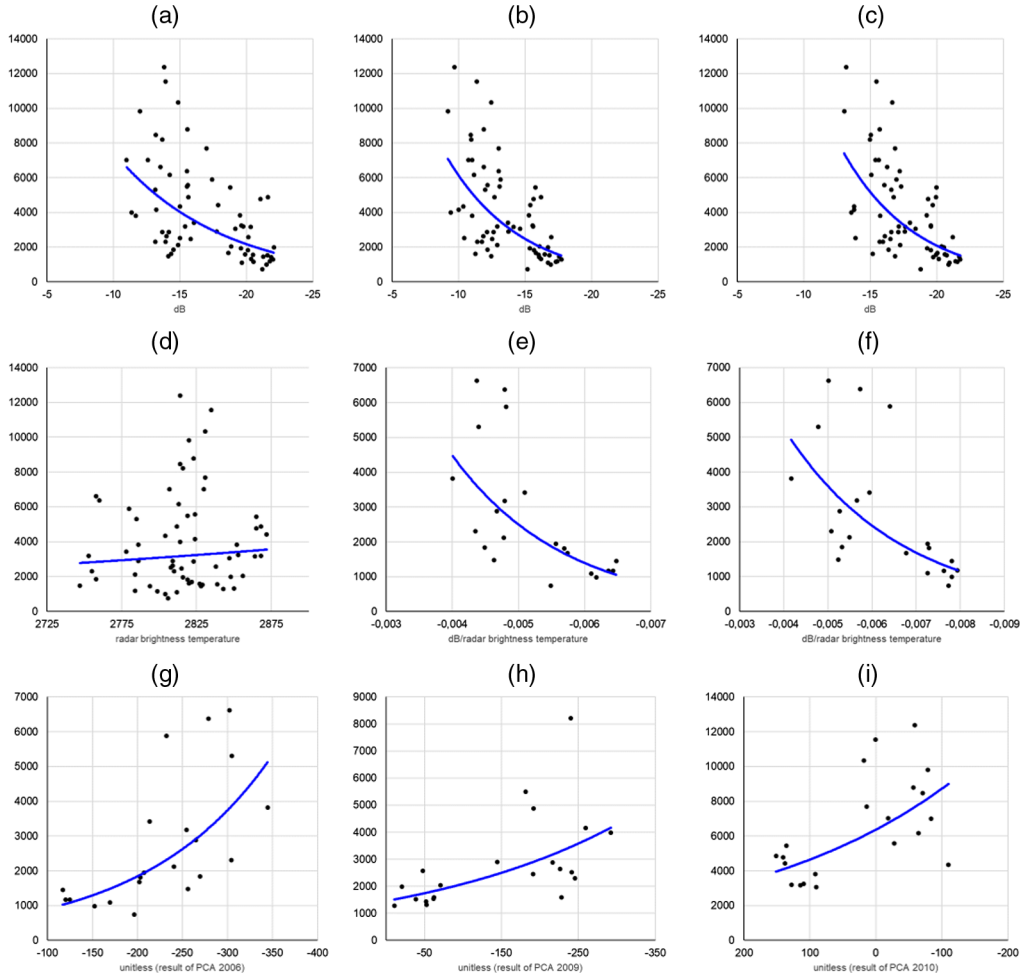

Fig. 1 Scatter plots of linear correlations between AGB [kg/ha] (*y*-axis) and radar variables (*x*-axis) as shown in Table 2.

the regression line captures both low and high values to a better degree. Accordingly, the capability of ALOS to predict large AGB values combined with the large-scale information of SSM/I is a suitable combination for savanna landscapes consisting of both trees and grasslands. It has to be noted that they are based on horizontal polarization images of December 2006 only because this was the only year when horizontal polarizations were available for all three sensors. Accordingly, the high correlation might result from the reduced number of samples but also could indicate that estimates benefit from uniform polarization characteristics.

The highest coefficient of determination was achieved for the PCA of the year 2006 ($R^2_{cd} = 0.515$), while the correlations of the PCAs of the other 2 years were distinctively lower. PCAs of the years 2009 and 2010 produced significantly lower R^2_{cd}. This can be partially explained by the distribution of samples in the scatter plots: While plot h lacks a clear trend and has larger outliers, samples were nearly split into two populations in plot i. The description of both distributions by an exponential function was not successful. As later shown in the prediction maps in Fig. 2, this resulted in an underestimation of high AGB values in case h and an overestimation in case i. This leads to the conclusion that, if suitable configurations and measurements without outliers are present, merging active and passive SAR information via PCA can lead to very high correlations. If there are inconsistencies in either the microwave imagery or the measured AGB, merging sensors might not improve the result compared with single-sensor correlations. Another possible reason for the different accuracies between these three years could be that SSM/I data from 2006 were acquired at a wavelength of 85 GHz, whereas the data from 2009 and 2010 was only available at 91 GHz.

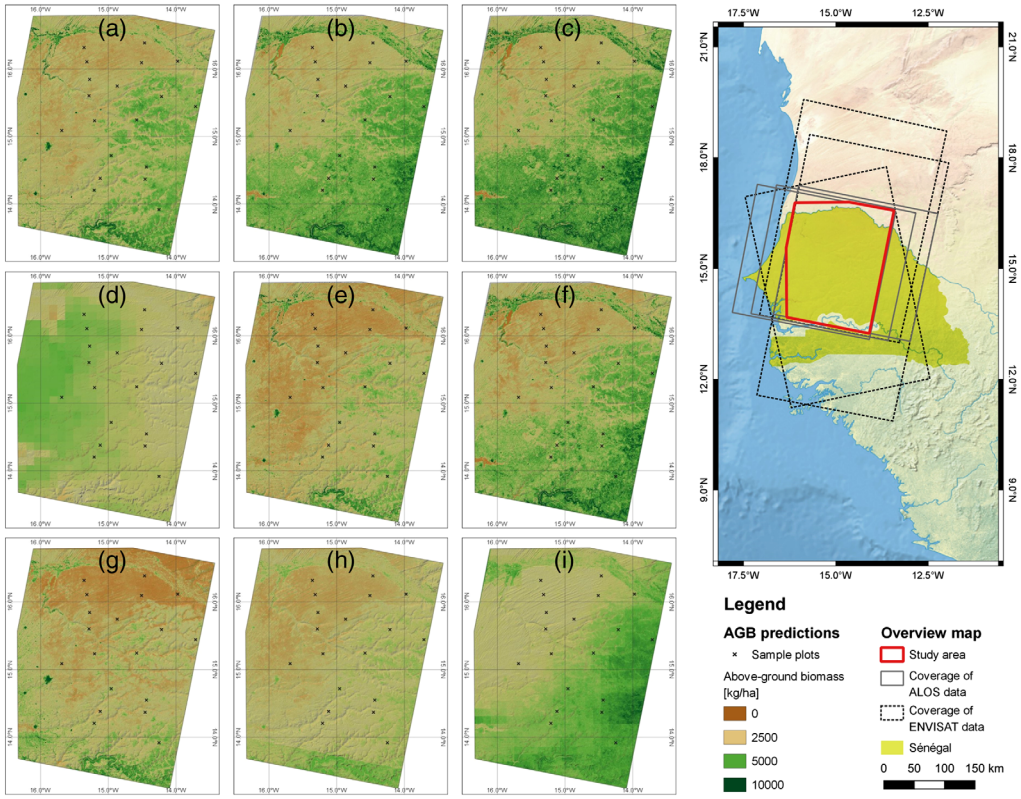

Fig. 2 Spatial prediction of AGB in the study area (marked red in the overview map). The letters refer to the equations in Table 2, which were based on different combinations of the used radar images.

3.2 *Spatial Prediction of Above-Ground Biomass*

The regressions shown in Table 2 were applied to the whole study area using the input rasters as variables in a raster calculator. Accordingly, the resulting AGB predictions (Fig. 2) show biomass variations at the detail level of the sensor with the highest spatial resolution, while still containing contributions from other sensor's variations involved in the regression. The maps support the indications made above that microwave information can generally be a very suitable proxy for the spatial distribution of biomass, even in sparsely vegetated areas. The low biomass areas in the northern center of the study area coincide with the Ferlo rangelands, a pastoral savanna with variable rainfall, and lack of permanent water availability.[76] Highest AGB values are found along the Sénégal river along the border between Sénégal and Mauritania, as well as in the denser savannas in the Tambacounda region of in the subhumid south.[77] Although all maps show similar patterns, it is also evident that some of them tend to overestimate or underestimate the measured biomass. Although the purely SAR-based estimates (maps a, b, and c) lie within a similar range of values, especially the measurements that involve SMM/I predict generally lower AGB values in the study area, especially maps e and g, respectively. Map i can be considered a special case because no clear trend between the sampled data for 2010 and the microwave observations was found [see Fig. 2(i)] and a large proportion of samples is clearly underestimated by the regression.

3.3 *Validation*

Because of the limitations regarding data availability of both satellite and field data, no independent validation could be performed based on points that were not used in the regressions. As a consequence of the limited sample size ($n = 21$ for some cases) and the required trade-off between bias and variance inherent in our data, we selected leave-one-out cross validation

over a k-fold cross validation.[78,79] The results are shown in Table 2 in the columns R^2_{val} and root mean square errors (RMSE). Compared with a 10-fold cross validation, leave-one-out produced significantly lower $R^2 s$, but the RMSE of between 1500 and 2500 kg per hectare were similarly estimated. Compared with the scatter plots in Fig. 1, the validation scores might be a bit pessimistic, yet we considered leave-one-out the more suitable and honest measure regarding the sample size and distribution of our data.[80] One major thing to note is that the lowest RMSEs are produced by the regressions based on both active and passive radar images. This furthermore underlines the potential of passive radar data to be integrated into AGB predictions, despite its significantly lower spatial resolution.

It became evident in this study that the availability of a sufficient number of representative samples is essential for a robust validation of the models. Having the samples split-up into independent training and testing subsets would clearly increase the robustness of the validation scores and finally increase the significance of the study.

3.4 *Discussion*

This study showed how satellite microwave imagery can be used to estimate AGB over large areas. Although most studies focus on tropical forest biomass, the estimates in ecosystems of low primary productivity, such as savannas or grasslands of the African Sahel zone, are still underrepresented in the literature. Our findings show good correlations with explained variances between 0.31 and 0.52, respectively. Accordingly, the combination of radar information from active and passive sensors can introduce high potentials because different types of scattering mechanisms and surface emittance are combined. This might be of particular interest for sub-Saharan countries, which often consist of a wide range of climate zones along their latitudinal gradient. The contribution of passive radar brightness temperature on the estimation quality of AGB is indicated by selected results, but clearly more research has to be carried out to prove its large-scale applicability.

Although the PCA of the year 2006 reached the highest R^2s in this study which partially confirms our hypothesis that combinations of active and passive radar, as well as short and long wavelength SAR data, lead to increased accuracies, the scores of the PCAs of 2009 and 2010 were significantly lower. We identified two possible reasons for this. First, the temporal difference between the acquisition of ALOS and ENVISAT is the shortest for 2006 (see 1), which reduces phenological variations and potentially leads to illtrained regressions. Second, negative western Sahelian rainfall anomalies were reported for the year 2006, leading to a more pronounced seasonality and therefore more distinct vegetation patterns.[81] Despite the promising results, we identified several points of concern to mention: starting with data selection, the temporal gap between the data collection (September and October) and the utilized radar imagery (November and December) was unavoidable because of unavailability of both ENVISAT and ALOS imagery at an earlier point of the investigated years. Yet, we see little potential for larger errors as the rainy season lasts until November in the northwest and the starting of the dry season has no immediate effect on aboveground vegetation.[82] It should still be attempted to keep the image acquisitions as close to the field measurements as possible.

Another critical point is the extreme difference in pixel sizes of active and passive radar data. This discrepancy has been lowered by averaging SAR backscatter within a radius of 1.5 km around each sampling sites, thus reducing the impact of extreme values on the regression. In case of speckle, this might be desirable, but as shown in Fig. 1, underestimation of high AGB values was a general problem and it could partially its origin here.

Furthermore, the combination of SAR bands of both horizontal and vertical polarization is not ideal. Whenever possible, X/C-band and L-band of the same polarization should be combined to make the best use of their complementary information. The missions of Sentinel-1 and ALOS-2, which were both launched in 2014, might serve as an ideal constellation as they both acquire images at regular intervals and with extensive coverage.

Due to the limited number of reference data collected in the field, a robust validation was not possible and the temporal difference between sampling and image acquisition was comparably large. For future studies, we pledge systematic field campaigns that take stratified and spatially representative samples and are aligned with the observation plans of the respective satellite

missions. This could clearly reduce the error caused by phenological dynamics.[83] As a consequence of the limitations described above, it can also be expected that the different number of samples used for the regression had an impact on its R^2, as well as the number of outliers. This again supports the necessity of a well-considered study design.

4 Conclusion and Outlook

Our approach showed that there are also good correlations between spaceborne SAR backscatter and low biomass conditions, which have values below 10 t/ha. However, our regressions showed clear underestimations for values above 5 t/ha. A statistical evaluation on the range and distribution of the collected AGB values is needed to select the suitable regression technique. While we used an exponential model to fit the data distribution, other cases might be more successful with linear, logarithmic, or multivariate techniques, as the logarithmic nature of the relationship between AGB and radar backscatter has often been demonstrated.[25]

Future SAR missions bring large potential regarding the multifrequency prediction of AGB: in addition to the missions of Sentinel-1 and ALOS-2 mentioned above, high-resolution SAR satellites are planned which fulfill both the criteria of large wavelengths (TanDEM-L, NovaSAR-S[84,85]) and temporal resolution (ICEYE-1[86]) to complement long-term passive radar missions. Despite the limitations of this study, we want to encourage other researchers to include passive radar information in biomass estimates and to further develop methods for areas with low primary production because there is a large need in monitoring seasonal variations and effects of climate changes on these systems.[87–89]

Acknowledgments

The authors thank the Centre de Suivi Écologique CSE (Dakar / Sénégal) for collecting and providing the biomass data and Edward Cahill for language editing of the manuscript. This study was funded by the Austrian Research Promotion Agency (FFG) under the Austrian Space Applications Programme (ASAP 12, 854041). ALOS data were provided by Japan Aerospace Exploration Agency (JAXA) within RA-6 (PI3059). ENVISAT data were provided by the European Space Agency (ESA). SSM/I data were provided by the National Snow and Ice Data Center (NSIDC). The authors declare no conflict of interest.

References

1. D. Lu, "The potential and challenge of remote sensing-based biomass estimation," *Int. J. Remote Sens.* **27**(7), 1297–1328 (2006).
2. P. C. Doraiswamy et al., "Crop yield assessment from remote sensing," *Photogramm. Eng. Remote Sens.* **69**(6), 665–674 (2003).
3. L. Serrano, I. Filella, and J. Penuelas, "Remote sensing of biomass and yield of winter wheat under different nitrogen supplies," *Crop Sci.* **40**(3), 723–731 (2000).
4. S. B. Idso, R. D. Jackson, and R. J. Reginato, "Remote-sensing of crop yields," *Science* **196**(4285), 19–25 (1977).
5. E. T. Mitchard et al., "Measuring biomass changes due to woody encroachment and deforestation/degradation in a forest–savanna boundary region of Central Africa using multitemporal l-band radar backscatter," *Remote Sens. Environ.* **115**(11), 2861–2873 (2011).
6. D. Boyd and F. Danson, "Satellite remote sensing of forest resources: three decades of research development," *Prog. Phys. Geog.* **29**(1), 1–26 (2005).
7. G. M. Foody, "Remote sensing of tropical forest environments: towards the monitoring of environmental resources for sustainable development," *Int. J. Remote Sens.* **24**(20), 4035–4046 (2003).
8. S. S. Saatchi et al., "Benchmark map of forest carbon stocks in tropical regions across three continents," *Proc. Natl. Acad. Sci. U. S. A.* **108**(24), 9899–9904 (2011).
9. T. Le Toan et al., "Relating radar remote sensing of biomass to modelling of forest carbon budgets," *Clim. Change* **67**(2–3), 379–402 (2004).

10. J. Dong et al., "Remote sensing estimates of boreal and temperate forest woody biomass: carbon pools, sources, and sinks," *Remote Sens. Environ.* **84**(3), 393–410 (2003).
11. S. M. Herrmann and T. K. Sop, "The map is not the territory: how satellite remote sensing and ground evidence have re-shaped the image of sahelian desertification," in *The End of Desertification?*, pp. 117–145, Springer, Berlin, Heidelberg (2016).
12. S. M. Herrmann, A. Anyamba, and C. J. Tucker, "Recent trends in vegetation dynamics in the African Sahel and their relationship to climate," *Global Environ. Change* **15**(4), 394–404 (2005).
13. A. Diouf and E. Lambin, "Monitoring land-cover changes in semi-arid regions: remote sensing data and field observations in the Ferlo, Senegal," *J. Arid Environ.* **48**(2), 129–148 (2001).
14. H. Eswaran, E. Van Den Berg, and P. Reich, "Organic carbon in soils of the world," *Soil Sci. Soc. Am. J.* **57**(1), 192–194 (1993).
15. J. Anderson, "The effects of climate change on decomposition processes in grassland and coniferous forests," *Ecol. Appl.* **1**(3), 326–347 (1991).
16. C. Ryan et al., "Carbon losses from deforestation and widespread degradation offset by extensive growth in African Woodlands," *Nat. Commun.* **9**, 3045 (2018).
17. D. O. Hall and J. Scurlock, "Climate change and productivity of natural grasslands," *Ann. Bot.* **67**(Supp1), 49–55 (1991).
18. J. A. Richards, G.-Q. Sun, and D. S. Simonett, "L-band radar backscatter modeling of forest stands," *IEEE Trans. Geosci. Remote Sens.* **GE-25**(4), 487–498 (1987).
19. A. E. Stovall and H. H. Shugart, "Improved biomass calibration and validation with terrestrial LIDAR: implications for future LIDAR and SAR missions," *IEEE J. Sel. Top. Appl. Earth Obs. Remote Sens.* **11**(10), 3527–3537 (2018).
20. E. T. Mitchard et al., "Using satellite radar backscatter to predict above-ground woody biomass: a consistent relationship across four different African landscapes," *Geophys. Res. Lett.* **36**(23), L23401 (2009).
21. A. Luckman et al., "A study of the relationship between radar backscatter and regenerating tropical forest biomass for Spaceborne SAR instruments," *Remote Sens. Environ.* **60**(1), 1–13 (1997).
22. G. M. Foody et al., "Observations on the relationship between sir-c radar backscatter and the biomass of regenerating tropical forests," *Int. J. Remote Sens.* **18**(3), 687–694 (1997).
23. Y. Rauste et al., "Radar-based forest biomass estimation," *Int. J. Remote Sens.* **15**(14), 2797–2808 (1994).
24. M. C. Dobson et al., "Dependence of radar backscatter on coniferous forest biomass," *IEEE Trans. Geosci. Remote Sens.* **30**(2), 412–415 (1992).
25. N. Joshi et al., "Understanding saturation of radar signals over forests," *Sci. Rep.* **7**(1), 3505 (2017).
26. M. L. Imhoff, "Radar backscatter/biomass saturation: observations and implications for global biomass assessment," in *Int. Geoscience and Remote Sensing Symp. (IGARSS'93)*, IEEE, pp. 43–45 (1993).
27. T. Mette et al., "Forest biomass estimation using polarimetric SAR interferometry," in *Int. Geoscience and Remote Sensing Symp. (IGARSS'02)*, IEEE, Vol. 2, pp. 817–819 (2002).
28. S. Englhart, V. Keuck, and F. Siegert, "Aboveground biomass retrieval in tropical forests–the potential of combined x-and l-band SAR data use," *Remote Sens. Environ.* **115**(5), 1260–1271 (2011).
29. M. Cutler et al., "Estimating tropical forest biomass with a combination of SAR image texture and landsat TM data: an assessment of predictions between regions," *ISPRS J. Photogramm. Remote Sens.* **70**, 66–77 (2012).
30. G. Sun et al., "Forest biomass mapping from LIDAR and Radar synergies," *Remote Sens. Environ.* **115**(11), 2906–2916 (2011).
31. S. Solberg et al., "Estimating spruce and pine biomass with interferometric x-band SAR," *Remote Sens. Environ.* **114**(10), 2353–2360 (2010).
32. X. Tian et al., "Estimation of forest above-ground biomass using multi-parameter remote sensing data over a cold and arid area," *Int. J. Appl. Earth Obs. Geoinf.* **14**(1), 160–168 (2012).

33. T. Svoray and M. Shoshany, "Herbaceous biomass retrieval in habitats of complex composition: a model merging SAR images with unmixed landsat TM data," *IEEE Trans. Geosci. Remote Sens.* **41**(7), 1592–1601 (2003).
34. T. Svoray and M. Shoshany, "Sar-based estimation of areal aboveground biomass (aab) of herbaceous vegetation in the semi-arid zone: a modification of the water-cloud model," *Int. J. Remote Sens.* **23**(19), 4089–4100 (2002).
35. B. L. Foster et al., "Effects of hay management and native species sowing on grassland community structure, biomass, and restoration," *Ecol. Appl.* **19**(7), 1884–1896 (2009).
36. T. Le Toan et al., "The biomass mission: mapping global forest biomass to better understand the terrestrial carbon cycle," *Remote Sens. Environ.* **115**(11), 2850–2860 (2011).
37. C. Finnigan, "Developing a grassland biomass monitoring tool using a time series of dual polarimetric SAR and optical data," PhD thesis (2013).
38. M. Shimada et al., "Generation of 10 m resolution PALSAR and JERS-1 SAR mosaic and forest/non-forest maps for forest carbon tracking," in *3rd Int. Asia-Pacific Conf. on Synthetic Aperture Radar (APSAR)*, IEEE, pp. 1–4 (2011).
39. Y. Rauste, "Multi-temporal JERS SAR data in boreal forest biomass mapping," *Remote Sens. Environ.* **97**(2), 263–275 (2005).
40. A. Luckman et al., "Tropical forest biomass density estimation using JERS-1 SAR: seasonal variation, confidence limits, and application to image mosaics," *Remote Sens. Environ.* **63**(2), 126–139 (1998).
41. R. Hagensieker and B. Waske, "Evaluation of multi-frequency SAR images for tropical land cover mapping," *Remote Sens.* **10**(2), 257 (2018).
42. H. Omar, M. A. Misman, and A. R. Kassim, "Synergetic of PALSAR-2 and sentinel-1a SAR polarimetry for retrieving aboveground biomass in dipterocarp forest of Malaysia," *Appl. Sci.* **7**(675), 1–20 (2017).
43. S. Englhart et al., "Modeling aboveground biomass in tropical forests using multi-frequency SAR data—a comparison of methods," *IEEE J. Sel. Top. Appl. Earth Obs. Remote Sens.* **5**(1), 298–306 (2012).
44. H. S. Srivastava et al., "Multi-frequency and multi-polarized SAR response to thin vegetation and scattered trees," *Curr. Sci.* **97**(3), 425–429 (2009).
45. M. Herold, C. Schmullius, and I. Hajnsek, "Multifrequency and polarimetric radar remote sensing of grassland-geobiophysical and landcover parameter retrieval with e-SAR data," in *20th Annual Symp. of the European-Association-of-Remote-Sensing-Laboratories (EARSeL)*, pp. 95–102 (2001).
46. S. Paloscia et al., "A multifrequency algorithm for the retrieval of soil moisture on a large scale using microwave data from SMMR and SSM/I satellites," *IEEE Trans. Geosci. Remote Sens.* **39**(8), 1655–1661 (2001).
47. J. T. Pulliainen, J. Grandell, and M. T. Hallikainen, "Retrieval of surface temperature in boreal forest zone from SSM/I data," *IEEE Trans. Geosci. Remote Sens.* **35**(5), 1188–1200 (1997).
48. P. Ferrazzoli et al., "Sensitivity to microwave measurements to vegetation biomass and soil moisture content: a case study," *IEEE Trans. Geosci. Remote Sens.* **30**(4), 750–756 (1992).
49. K. B. Eom, "Unsupervised segmentation of spaceborne passive Radar images," *Pattern Recognit. Lett.* **20**(5), 485–494 (1999).
50. Y. Y. Liu et al., "Recent reversal in loss of global terrestrial biomass," *Nat. Clim. Change* **5**(5), 470–474 (2015).
51. R. Armstrong et al., *DMSP SSM/I-SSMIS Pathfinder Daily Ease-Grid Brightness Temperatures. Version 2*, NASA National Snow Ice Data Center Distributed Active Archive Center, Boulder, Colorado (1994).
52. P. S. Poissonet et al., "A comparison of sampling methods in dense herbaceaous pasture," *J. Range Manage.* **26**(1), 65–67 (1973).
53. G. Yameogo et al., "Méthodologie de collectes des données de la biomasse herbacée et ligneuse. impact environmental du pngt 2: suivi du couvert végétal," 2004, Ministry of Agrigulture, Ouagadougou, Burkina Faso, http://www.beep.ird.fr/collect/pngt2/index/assoc/HASH1d5f.dir/Methodologie%20de%20collecte%20des%20donnee.pdf (15 November 2018).

54. R. Kindt et al., "Useful tree species for Africa: interactive vegetation maps and species composition tables based on the vegetation map of Africa," Report, World Agroforestry Centre, Nairobi, Kenya (2011).
55. P. Hejcmanovā-Nežerková and M. Hejcman, "A canonical correspondence analysis (CCA) of the vegetation–environment relationships in Sudanese Savannah, Senegal," *S. Afr. J. Bot.* **72**(2), 256–262 (2006).
56. M. I. Cissé et al., "The browse production of some trees of the Sahel: relationships between maximum foliage biomass and various physical parameters," in *Browse in Africa*, H. N. le Houerou's et al., Ed., pp. 205–210, International Livestock Centre for Africa, Addis Ababa, Ethiopia (1980).
57. F. Rembold et al., "Agricultural drought monitoring using space-derived vegetation and biophysical products: a global perspective," in *Remote Sensing of Water Resources, Disasters, and Urban Studies*, P. S. Thenkabail, Ed., pp. 349–365, CRC Press, Boca Raton (2015).
58. F. Ham and E. Fillol, "Pastoral surveillance system and feed inventory in the Sahel," in *Conducting National Feed Assessments*, M. B. Coughenour and H. P. Makkar, Eds., pp. 83–94, Food and Agriculture Organization of the United Nations (FAO), Rome, Italy (2012).
59. P. A. Moran, "Notes on continuous stochastic phenomena," *Biometrika* **37**(1/2), 17–23 (1950).
60. J.-B. Henry et al., "ENVISAT multi-polarized ASAR data for flood mapping," *Int. J. Remote Sens.* **27**(10), 1921–1929 (2006).
61. M. Shimada et al., "Palsar radiometric and geometric calibration," *IEEE Trans. Geosci. Remote Sens.* **47**(12), 3915–3932 (2009).
62. A. Jarvis et al., "Hole-filled seamless SRTM data V4," 2008, International Centre for Tropical Agriculture (CIAT), Cali, Colombia, http://srtm.csi.cgiar.org/ (15 November 2018).
63. D. Small, "Flattening gamma: radiometric terrain correction for SAR imagery," *IEEE Trans. Geosci. Remote Sens.* **49**(8), 3081–3093 (2011).
64. L. Pierce et al., "Practical SAR orthorectification," in *Int. Geoscience and Remote Sensing Symp. (IGARSS '96)*, IEEE, Vol. 4, pp. 2329–2331 (1996).
65. F. J. Wentz, "SSM/I version-7 calibration report," Report Number 11012, p. 46, Remote Sensing Systems, Santa Rosa, California (2013).
66. J. P. Hollinger, J. L. Peirce, and G. A. Poe, "SSM/I instrument evaluation," *IEEE Trans. Geosci. Remote Sens.* **28**(5), 781–790 (1990).
67. R Core Team, *R: A Language and Environment for Statistical Computing*, R Foundation for Statistical Computing, Vienna, Austria (2018).
68. S. Baig et al., "Above ground biomass estimation of dalbergia sissoo forest plantation from dual-polarized ALOS-2 PALSAR data," *Can. J. Remote Sens.* **43**(3), 297–308 (2017).
69. M. A. Stelmaszczuk-Górska et al., "Estimation of above-ground biomass over boreal forests on siberia using updated in situ, ALOS-2 PALSAR-2, and RADARSAT-2 data," *Remote Sens.* **10**(10), 1550 (2018).
70. J. Smith et al., "A comparison of the effects of resampling before and after classification on the accuracy of a landsat derived cover type map," in *Proc. of Int. Conf. on the Remote Sensing Society and the Centre for Earth Resources Management*, pp. 391–400 (1985).
71. S. Peleg, M. Werman, and H. Rom, "A unified approach to the change of resolution: space and gray-level," *IEEE Trans. Pattern Anal. Mach. Intell.* **11**(7), 739–742 (1989).
72. C. Justice et al., "Spatial degradation of satellite data," *Int. J. Remote Sens.* **10**(9), 1539–1561 (1989).
73. C. Pohl and J. L. Van Genderen, "Review article multisensor image fusion in remote sensing: concepts, methods and applications," *Int. J. Remote Sens.* **19**(5), 823–854 (1998).
74. J.-S. Lee, M. R. Grunes, and E. Pottier, "Quantitative comparison of classification capability: fully polarimetric versus dual and single-polarization SAR," *IEEE Trans. Geosci. Remote Sens.* **39**(11), 2343–2351 (2001).
75. S.-T. Wu and S. A. Sader, "Multipolarization SAR data for surface feature delineation and forest vegetation characterization," *IEEE Trans. Geosci. Remote Sens.* **GE-25**(1), 67–76 (1987).

76. H. K. Adriansen and T. T. Nielsen, "Going where the grass is greener: on the study of pastoral mobility in Ferlo, Senegal," *Hum. Ecol.* **30**(2), 215–226 (2002).
77. C. Mbow, T. T. Nielsen, and K. Rasmussen, "Savanna fires in east-central senegal: distribution patterns, resource management and perceptions," *Hum. Ecol.* **28**(4), 561–583 (2000).
78. Y. Zhang and Y. Yang, "Cross-validation for selecting a model selection procedure," *J. Econometrics* **187**(1), 95–112 (2015).
79. Y. Bengio and Y. Grandvalet, "No unbiased estimator of the variance of k-fold cross-validation," *J. Mach. Learn. Res.* **5**(Sep), 1089–1105 (2004).
80. D. M. Bates and D. G. Watts, *Nonlinear Regression Analysis and its Applications*, John Wiley & Sons, Inc., New York (1988).
81. S. Janicot et al., "Large-scale overview of the summer monsoon over West Africa during the amma field experiment in 2006," *Ann. Geophys.* **26**, 2569–2595 (2008).
82. S. Cissé et al., "Rainfall intra-seasonal variability and vegetation growth in the Ferlo Basin (Senegal)," *Remote Sens*. **8**(1), 66 (2016).
83. S. L. Powell et al., "Quantification of live aboveground forest biomass dynamics with Landsat time-series and field inventory data: a comparison of empirical modeling approaches," *Remote Sens. Environ.* **114**(5), 1053–1068 (2010).
84. A. Moreira et al., "TanDEM-L: a highly innovative bistatic SAR mission for global observation of dynamic processes on the earth's surface," *IEEE Geosci. Remote Sens. Mag.* **3**(2), 8–23 (2015).
85. M. Cohen et al., "NOVASAR-S low cost Spaceborne SAR payload design, development and deployment of a new benchmark in Spaceborne Radar," in *IEEE Radar Conf. (RadarConf)*, pp. IEEE, 0903–0907 (2017).
86. Y. Sugimoto, S. Ozawa, and N. Inaba, "Spaceborne synthetic aperture radar signal processing using field-programmable gate arrays," *J. Appl. Remote Sens.* **12**(3), 035007 (2018).
87. J. A. Tambo and T. Abdoulaye, "Smallholder farmers' perceptions of and adaptations to climate change in the Nigerian Savanna," *Reg. Environ. Change* **13**(2), 375–388 (2013).
88. A. D. Richardson et al., "Climate change, phenology, and phenological control of vegetation feedbacks to the climate system," *Agric. For. Meteorol.* **169**, 156–173 (2013).
89. W. Parton et al., "Impact of climate change on grassland production and soil carbon worldwide," *Global Change Biol.* **1**(1), 13–22 (1995).

Andreas Braun is a researcher in the Department for Geography, University of Tübingen, where he received his BSc and MSc degrees in physical geography in 2010 and 2014, respectively. His PhD thesis deals with the application of synthetic aperture radar imagery in for humanitarian response. Furthermore, he works on the analysis of landscape systems and the assistance of urban planning by methods of earth observation.

Julia Wagner received her MSc degree in physical geography from the University of Tübingen in 2017. Since 2018, she has been a PhD student in the Department for Physical Geography, Stockholm University. Her PhD project deals with the analysis of permafrost regions using different remote sensing techniques.

Volker Hochschild is a professor in the Department for Geography, University of Tübingen. His research focus is remote sensing for landscape analysis and hydrology, geographic information systems and web-based geodatabases. He authored numerous peer-reviewed scientific papers and is involved in several national and international research projects. He is a reviewer for various IEEE journals and the *Journal of Geomorphology and Environmental Modelling*.